in: Proc. of the Workshop on Crystalline Ion Beams, Wertheim, W. Germany, Ed. by R. W. Hasse, I. Hofmann, D. Liese (GSI report GSI-89-10, ISSN 0170-4546), p. 241.

Coulomb Clusters of Ions in a Paul Trap*

Wayne M. Itano J. C. Bergquist D. J. Wineland

Time and Frequency Division
National Institute of Standards and Technology
(formerly National Bureau of Standards)
Boulder, Colorado 80303, U.S.A.

Abstract

Ordered structures of as many as 16 laser-cooled Hg^+ ions, confined in a Paul trap, have been observed. These structures, called Coulomb clusters, match those calculated by minimizing the effective potential energy of the system. The $5d^{10}6s\ ^2S_{1/2}$ to $5d^96s^2\ ^2D_{5/2}$ transition in Hg^+ has been observed by optical-optical double resonance. The resolution was high enough that Doppler-induced sidebands, due to the harmonic motion of a single ion in the trap, were clearly resolved. Additional sidebands, due to the relative vibration of two ions forming a pseudomolecule, have also been observed.

I. Introduction

A group of a few ions in a Paul (radiofrequency) trap is a system that can be modelled with simple calculations, but which still exhibits phenomena, such as spatial ordering and phase transitions, which are associated with condensed matter. Stimulated in part by recent theoretical predictions that systems of laser-cooled ions would form spatially ordered structures,[1–5] several experimental groups have produced and studied such structures.[6–11]

We have created systems of a few Hg^+ ions, which we call Coulomb clusters, in which the positions of the ions are approximately fixed relative to each other. These relative positions are determined by a balance between the confining forces of the trap and the mutual Coulomb repulsion of the ions. We have also observed a modification of the optical absorption spectrum of the ions by the harmonic vibration of two ions relative to each other. This vibration is an indication that the ions have formed a spatially ordered state. Direct evidence of spatial ordering has been obtained by two-dimensional imaging of the laser-induced fluorescence from the ions. Images of up to 16 ions have been recorded and compared with calculations. These clusters are a novel form of matter, in which the spacing between atoms is larger by about three orders of magnitude than in an ordinary crystal or molecule. Observations of similar structures of ions in a Penning trap have been made recently.[12] Those structures

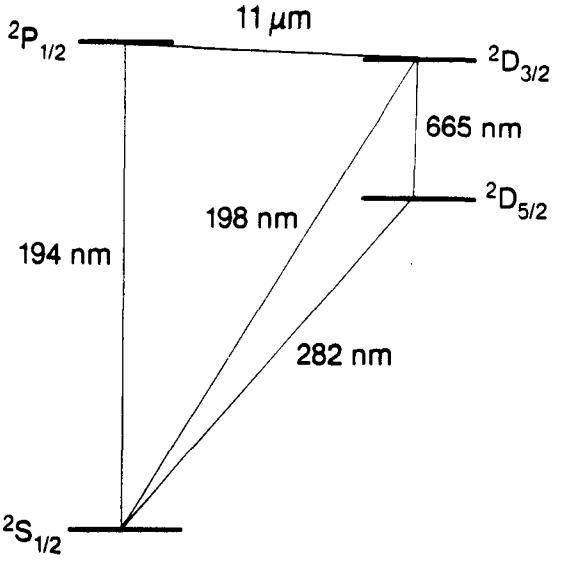

Figure 1: The lowest energy levels of Hg^+.

contained more ions than those described here (as many as 15 000). However, individual ions were not resolved in the Penning trap, as they were in the Paul trap. The smallest clusters studied in the Penning trap had about 20 ions, so that the two experiments taken together cover a range of ion numbers from one to 15 000. We have also observed Coulomb clusters of charged particles with diameters of several micrometers in a large Paul trap. Such clusters of mascroscopic particles are more easily produced and observed than ion clusters. However, the charge-to-mass ratio cannot be made as uniform as for ions. In Thomson's model of the atom, the potential energy function for the electrons was essentially the same as for the ions in a Paul trap. As a result, some of the cluster shapes that we observe are the same as those Thomson calculated for atomic electrons. Preliminary reports of this work have appeared elsewhere.[7,10]

II. Hg^+ levels

The lowest energy states of the mercury ion are shown in Fig. 1. The ground state is $^2S_{1/2}$, as in an alkali atom. The strong $^2S_{1/2}$ to $^2P_{1/2}$ electric dipole transition at 194 nm is used for the laser cooling and fluorescence detection. The lifetime of the $^2P_{1/2}$ state is about 2 ns. Usually, it decays directly back to the ground $^2S_{1/2}$ state. About once in 10^7 times, it decays instead to the metastable $^2D_{3/2}$ state, which has a lifetime of about 9 ms. If this happens the 194 nm fluorescence abruptly turns off. The $^2D_{3/2}$ state decays about half the time directly to the ground state and the rest of the time to the metastable $^2D_{5/2}$ state, which has a lifetime of about 86 ms. After the decay to the ground state the fluorescence turns on again. Thus, the 194 nm fluorescence from a single ion is bistable and switches randomly between zero and a steady level. The statistical properties of this bistable signal

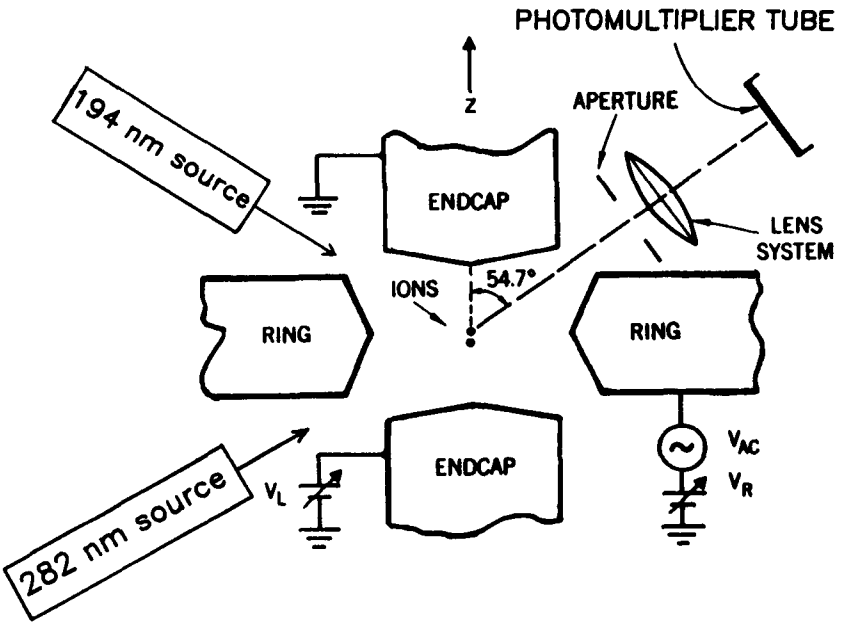

Figure 2: Schematic view of the apparatus. The separation between the endcap electrodes is approximately 625 μm. The inner diameter of the ring electrode is approximately 890 μm.

have been used to measure the decay rates of the metastable states.[13]

III. Apparatus

The experimental apparatus is shown schematically in Fig. 2. The electrodes of the Paul trap are shown in cross section. Radiofrequency and static voltages are applied between the electrodes to control the effective potential well for the ions. The 194 nm laser beam passes along a diagonal between the electrodes. The 194 nm source is required both for detecting the ions and for cooling them (by resonant radiation pressure). The 194 nm fluorescence is detected along another diagonal. For some experiments, the 194 nm detector is a photomultiplier tube. In other cases, a resistive-anode photomultiplier tube that provides two-dimensional positional information from single photoelectrons is used. For optical-optical double resonance experiments, 282 nm light from a frequency-doubled dye laser is focused on the ions.

A. Paul trap

The electric potential inside an ideal Paul trap is given by the expression,

$$\phi(x,y,z) = \frac{U_0 + V_0\cos(\Omega t)}{A^2}(x^2 + y^2 - 2z^2). \tag{1}$$

The potential V applied between the ring electrode and the two endcap electrodes is the sum of a static and a radiofrequency part: $V = U_0 + V_0\cos(\Omega t)$. The parameter A depends

on the geometry of the trap electrodes and has the dimensions of area. The radiofrequency voltage V_0 gives rise to an effective potential which confines in all directions. This potential is four times as strong in the axial (z) direction as in the radial (r) direction. The ratio of the axial to radial confining force can be changed by varying the static voltage U_0. The effective potential energy which governs the average motion, called the secular motion, is

$$q\phi_{\text{eff}}(x,y,z) = \left(\frac{q^2V_0^2}{m\Omega^2A^4} + \frac{qU_0}{A^2}\right)(x^2+y^2) + \left(\frac{4q^2V_0^2}{m\Omega^2A^4} - \frac{2qU_0}{A^2}\right)z^2 \quad (2)$$

$$= \frac{m\omega_r^2}{2}(x^2+y^2) + \frac{m\omega_z^2}{2}z^2. \quad (3)$$

We call the harmonic frequencies for the secular motion along the axial and radial directions ω_z and ω_r. The ion also oscillates at the frequency Ω of the applied field. This motion is called the micromotion. Under normal operating conditions, Ω is much greater than ω_z or ω_r. If there is a slight deviation from axial symmetry, we can describe the effective potential in terms of secular frequencies ω_x and ω_y, provided that we align the coordinate axes along the principal axes of the potential. The effective potential is

$$q\phi_{\text{eff}}(x,y,z) = \frac{m\omega_x^2}{2}x^2 + \frac{m\omega_y^2}{2}y^2 + \frac{m\omega_z^2}{2}z^2, \quad (4)$$

where $\omega_x \approx \omega_y$.

The trap used in these experiments has been described previously.[14] The electrodes were made of molybdenum. The design of the electrodes, which were machined with simple straight cuts, has been discussed in detail elsewhere.[15] The inside diameter of the ring electrode was less than 1 mm. This allowed very strong electric field gradients to be applied. The maximum value of V_0 was about 1 kV. The frequency $\Omega/2\pi$ was about 23 MHz. The ions were created inside the trap by electron impact ionization of isotopically purified ^{198}Hg.

B. Lasers

The cw, tunable 194 nm source has been described previously.[16] Radiation at 257 nm was generated by frequency doubling the output of a 515 nm single-mode cw argon ion laser in an ammonium dihydrogen phosphate crystal. This radiation was mixed with the output of a 792 nm cw dye laser in a potassium pentaborate crystal to generate the sum frequency at 194 nm. The efficiencies of the frequency doubling and mixing processes were enhanced by using ring buildup cavities to increase the powers of the input beams circulating through the crystals. About 5 μW were generated at 194 nm. The bandwidth was about 2 MHz.

The narrowband 282 nm source was obtained from a dye laser that was frequency doubled in a deuterated ammonium dihydrogen phosphate crystal. The bandwidth of the dye laser, which was stabilized to a Fabry-Perot cavity, was about 15 kHz for these experiments. Recently, the linewidth of this laser has been decreased further by stabilizing it to a higher-finesse cavity.

C. Photon imaging detection

A three-stage lens system projected an image of the ion fluorescence onto the photocathode of the position-sensitive photon counter with a magnification of about 180. The first stage

was an aberration-corrected multi-element lens with an f-number of 4.5. The positional information from single detected photons was available in either analog or digital form. Images could be observed in real time on an oscilloscope screen, using the analog pulses. The digital information went to a computer, in order to make time exposures. An image of a single ion in the trap, recorded with this apparatus, has been published previously.[17]

IV. High resolution optical spectroscopy

A. Optical-optical double resonance

We have observed the 282 nm $^2S_{1/2}$ to $^2D_{5/2}$ electric quadrupole transition with high resolution. The metastable $^2D_{5/2}$ state has a lifetime of about 86 ms, so the transition has a natural linewidth of about 2 Hz. It would be very difficult to observe this transition in a single ion by detecting the emitted 282 nm photons, since there would be at most about 11 photons per second. To increase the efficiency of observation, we use optical-optical double resonance with quantum amplification.[14,18,19] The method works in the following way. The 194 nm source is turned off and 282 nm source is turned on. Suppose the ion absorbs a 282 nm photon, and is put into the metastable state. When the 194 nm light is then turned on, no fluorescence is observed. If, on the other hand, the ion is still in the ground state when the 194 nm light is turned on, fluorescence is observed at the normal intensity (typically thousands of photons per second detected). After a few milliseconds, the state of the ion can be determined with almost complete certainty. This technique was developed with the goal of making an optical frequency standard. Here it is used to yield information about the temperature and mutual interactions of the trapped ions.

B. Single-ion motional sidebands

The Doppler broadening of an absorption resonance of an ion bound in a harmonic well is modified by the confinement.[20] Instead of a single, broadened resonance line, the spectrum takes the form of a series of discrete resonances, each having a width equal to the natural width of the resonance, which are separated by the frequency of harmonic motion.

Consider an ion moving in the x direction in a harmonic well with frequency ω_x and amplitude X_0, so that

$$x = X_0 \cos(\omega_x t). \tag{5}$$

Let it be irradiated by a monochromatic laser beam of frequency ω propagating along the x axis. The electric field $\vec{E}(x,t)$ of the laser beam is

$$\vec{E}(x,t) = \mathrm{Re}\ \vec{E}_0 e^{i(kx-\omega t)}, \tag{6}$$

where the symbol Re denotes the real part of a complex expression. In the frame of the ion, there is a frequency modulation of the laser field. The electric field in the ion's frame is obtained by substituting the expression for x given by Eq. (5) into Eq. (6):

$$\begin{aligned} \vec{E}(x,t) &= \mathrm{Re}\ \vec{E}_0 e^{i(kX_0 \cos\omega_x t - \omega t)} \\ &= \mathrm{Re}\ \vec{E}_0 \sum_{n=-\infty}^{+\infty} i^n J_n(kX_0) e^{-i(\omega - n\omega_x)t}. \end{aligned} \tag{7}$$

In addition to the carrier at ω, the ion sees sidebands, called motional sidebands, spaced by the harmonic oscillation frequency ω_x. The amplitudes of the sidebands are proportional to the Bessel functions J_n. The ion absorbs light when the laser frequency is equal to one of its resonance frequencies and also when one of the motional sidebands matches a resonance frequency.

The intensities of the sidebands can be used to measure the temperature of the ion. A quantum mechanical treatment, in which a thermal-state-probability distribution was assumed, has been given previously.[21] According to Eq. (44) of Ref. 21, the intensity of the nth sideband $\sigma(n)$, is

$$\sigma(n) = \sigma_0 \exp\left(\frac{n\hbar\omega_x}{2k_BT} - k^2\langle x^2\rangle\right) I_n\left(\exp\left(\frac{\hbar\omega_x}{k_BT}(kx_0)^2\langle n_x\rangle\right)\right). \tag{8}$$

In this notation, the intensity of the carrier is $\sigma(0)$, I_n is a modified Bessel function, and $\langle x^2\rangle$ is the mean squared displacement of the harmonic oscillator, given by

$$\langle x^2\rangle = \frac{\hbar}{m\omega_x}(\langle n_x\rangle + \tfrac{1}{2}) \equiv 2x_0^2(\langle n_x\rangle + \tfrac{1}{2}), \tag{9}$$

where m is the mass of the ion and $\langle n_x\rangle$ is the mean occupation number of the oscillator. The temperature T is related to $\langle n_x\rangle$ by

$$\langle n_x\rangle = \frac{1}{\exp\left(\frac{\hbar\omega_x}{k_BT}\right) - 1}. \tag{10}$$

Equation 8 can easily be generalized to cases where there are two or more distinct frequencies of motion and where the laser beam is not directed along one of the principal axes of the trap. We have measured the temperature of a single, laser-cooled Hg^+ ion from the motional sidebands of the $^2S_{1/2}$ to $^2D_{5/2}$ transition.[22] The measured temperature was about 2 mK, which agrees with theoretical predictions.[21]

Figure 3(a) shows the absorption spectrum of a single Hg^+ ion, observed by the optical-optical double resonance. The carrier (at optical frequency ν_0) and the motional sidebands above and below ν_0 are clearly resolved. The potentials U_0 and V_0 were adjusted so that $\nu_r \approx 2\nu_z \approx 473$ kHz, where $\nu_r \equiv \omega_r/2\pi$ and $\nu_z \equiv \omega_z/2\pi$. This condition helped to simplify the sideband spectrum. The frequencies ν_z and ν_r were determined experimentally by applying a radiofrequency voltage between the electrodes. When the frequency of the applied voltage matched one of the secular frequencies, the fluorescence decreased, due to heating of the ion. In our notation for the sidebands, $(3z, r+z)$, for example, denotes the two overlapping sidebands at the frequencies $\nu_0 + 3\nu_z$ and $\nu_0 + \nu_r + \nu_z$.

C. Two-ion motional sidebands

If $\nu_z < \nu_r$, two ions have the lowest possible potential energy when they are located on the z axis, at $z = \pm z_{\min}$, where $z_{\min} = (q^2/4m\omega_z^2)^{1/3}$. The normal-mode frequencies of vibration about the minimum of the potential have been calculated previously.[3,7,8] The center of mass of the two ions behaves like a particle of mass $2m$ and charge $2q$ and thus has the same

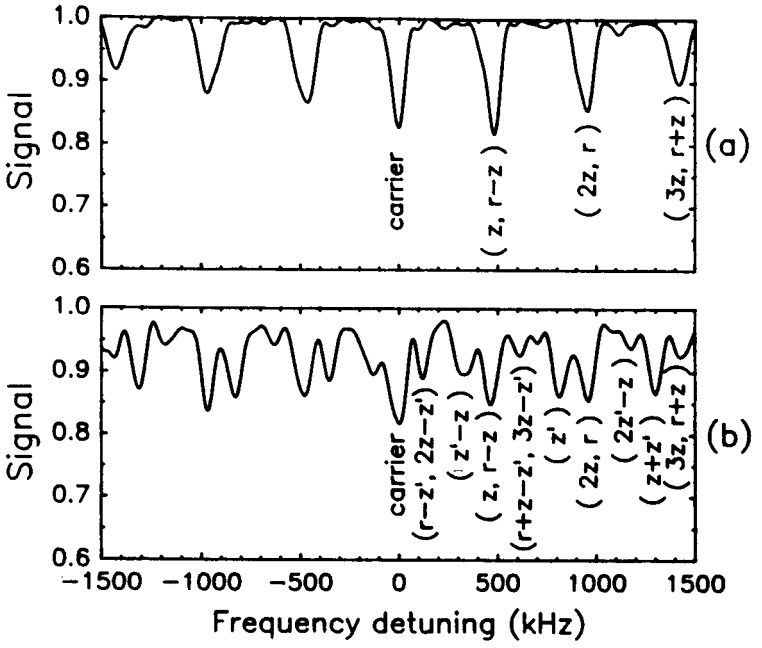

Figure 3: Absorption spectra of the $^2S_{1/2}(m_J = 1/2)$ to $^2D_{5/2}(m_J = -1/2)$ transition for (a) one Hg^+ ion and for (b) two Hg^+ ions. The carrier at optical frequency ν_0 (defined as zero frequency detuning) and the motional sidebands are clearly resolved. The sidebands are labeled in a notation that is explained in the text. The additional sidebands in (b) are due to the vibration of the two ions with respect to each other at frequency ν_z'.

frequencies of motion as a single ion. The frequency at which two ions vibrate with respect to each other along the z axis is $\nu_z' \equiv \sqrt{3}\nu_z$. This mode is like the stretch vibration of a diatomic molecule. The other vibrational frequency is $(\nu_r^2 - \nu_z^2)^{1/2}$, which, for $\nu_r = 2\nu_z$, is also equal to $\sqrt{3}\nu_z$. This vibration is a torsional motion in the x-z or y-z plane. Figure 3(b) shows an absorption spectrum taken with 2 ions in the trap. The trap potentials were the same as for the data of Fig. 3(a). The electronics of the position-sensitive photon detector were adjusted so that the fluorescence from only one of the two ions was detected. The motion of one ion is a superposition of harmonic motions at all of the normal-mode frequencies of the system. Therefore, all of the sidebands in Fig. 3(a) are also present in Fig. 3(b). The additional lines are due to the additional vibrational modes, at frequency ν_z', of the 2-ion pseudomolecule.

This kind of vibrational mode of two trapped ions has been observed by another method described in Ref. 9. Those workers applied a radiofrequency electric field between the trap electrodes, thus directly exciting the vibrational mode. When the frequency of the applied field matched the vibrational resonance, the fluorescence signal decreased.

V. Multi-ion cluster shapes

A. Calculations

The effective potential energy V_{eff} for a system of N ions of mass m and charge q is given by the expression,

$$V_{\text{eff}}(\{x_i, y_i, z_i\}) = \underbrace{\frac{m}{2}\sum_{i=1}^{N}(\omega_x^2 x_i^2 + \omega_y^2 y_i^2 + \omega_z^2 z_i^2)}_{\text{effective trap potential}} + \underbrace{\frac{1}{2}\sum_{i\neq j}\frac{q^2}{\mid \vec{r_i} - \vec{r_j} \mid}}_{\text{Coulomb repulsion}}. \tag{11}$$

Here, $\vec{r_i} = (x_i, y_i, z_i)$ is the position of the ith ion. The first term in Eq. (11) is the effective potential of the ions due to the trap fields. The second is the potential energy due to the Coulomb repulsion between the ions. The equilibrium configurations were calculated by finding the set of $3N$ ion coordinates that minimized the potential energy. A variable metric, or quasi-Newton, method was used to find the minimum, as in Ref. 3. We used the FORTRAN subroutine DFPMIN from Ref. 23. For a cylindrically symmetric Paul trap, there is an infinite set of solutions, since V_{eff} is unchanged by an arbitrary rotation about the z axis. To avoid possible convergence problems, and also to simulate the asymmetry of a real trap, ω_x and ω_y were assumed to differ by 0.2 %. Because of the remaining symmetry of the trap, there were in some cases several solutions, which were related by rotations and reflections. The algorithm sometimes converged to a minimum which was not the global minimum. In order to detect such false minima, at least 10 random initial configurations were used for each case. The solution with the lowest final value of V_{eff} was assumed to be a global minimum.

B. Observations

The ions were observed at an angle of approximately 54.7° with respect to the z axis of the trap. This allowed the three-dimensional structure of the clusters to be seen. In the apparatus of Ref. 6, the ions were observed along the z axis, so only the projection on the x-y plane could be seen. Figures 4-10 show the observed ion images and the corresponding calculated configurations. The magnification was the same for all of the experimental images. The scale of the experimental and calculated images is the same. The scale for the experimental images was determined from the separation between two ions, which is easily calculated. An approximate scale can be determined from the caption to Fig. 5. Experimental images of two, three, and four ions, obtained with less optical magnification, were published previously.[7]

Figure 4(a) shows five ions for $\nu_z = 0.308$ MHz and $\nu_r = 0.376$ MHz. Two of the ions lie along the z axis, symmetrically above and below the x-y plane. The other three ions circulate in the x-y plane about the z axis. They are not fixed in position, because the trap's effective potential is nearly cylindrically symmetric. Thus, the small, unintentional torque that the 194 nm beam applies to the system is enough to cause it to rotate. In this case, we determined the number of ions by reducing ν_z, relative to ν_r, until they were clearly separated in a chain along the z axis. Figure 4(b) shows the calculated ion positions for these

trap parameters. The circle in the calculated figure is obtained by rotating the configuration about the z axis.

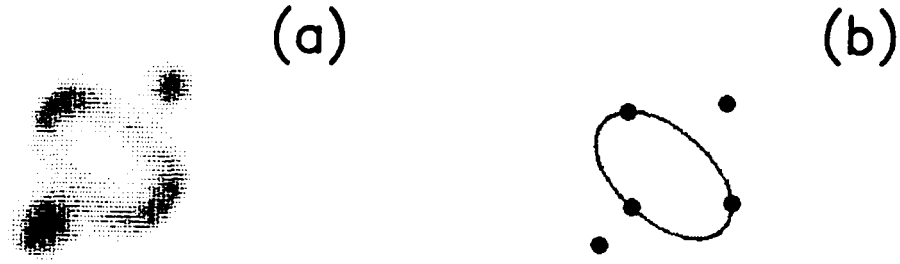

Figure 4: Nonplanar configuration of five ions for $\nu_z = 0.308$ MHz and $\nu_r = 0.376$ MHz. (a) Experimental data. (b) Calculation.

Figure 5 shows six ions for $\nu_z = 0.497$ MHz and $\nu_r = 0.256$ MHz. One is located at the origin. The other five circulate in the x-y plane. For these trap parameters, the configurations calculated for six, seven, and eight ions all have one ion at the origin and the rest in a ring in the x-y plane. In this case, we assume that there were six ions, because that number gives the best agreement between the observed and calculated ring sizes.

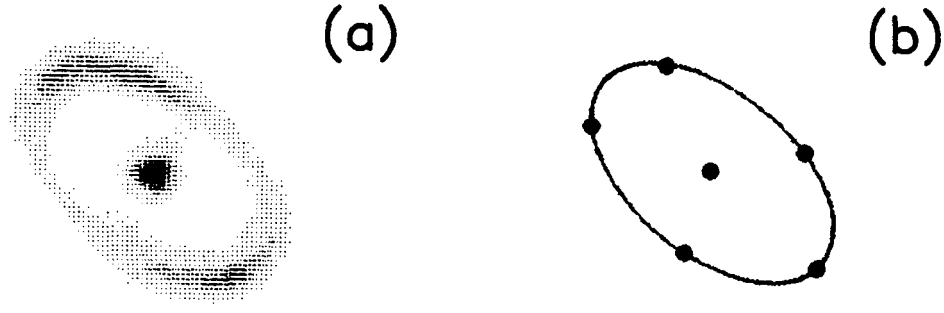

Figure 5: Planar configuration of six ions for $\nu_z = 0.497$ MHz and $\nu_r = 0.256$ MHz. The diameter of the ring is approximately 16 μm. (a) Experimental data. (b) Calculation.

Figure 6 shows six ions for $\nu_z = 0.780$ MHz and $\nu_r = 0.347$ MHz. One is at the origin, and four others lie at the vertices of a pentagon in the x-y plane. The fifth vertex of the pentagon appears to be vacant, but we assume that it is occupied by an ion which does not fluoresce. It may be a heavier isotope of mercury, such as $^{199}Hg^+$, or a molecular ion, such as $HgOH^+$, neither of which would fluoresce. If it had a higher charge-to-mass ratio than $^{198}Hg^+$, it would be more tightly bound to the trap, and would go the center. The additional asymmetry, due to the odd ion, keeps the configuration from rotating.

Figures 7 and 8 show two different configurations of the same nine ions. The secular frequencies for Fig. 7 were $\nu_z = 0.497$ MHz and $\nu_r = 0.256$ MHz; for Fig. 8, they were

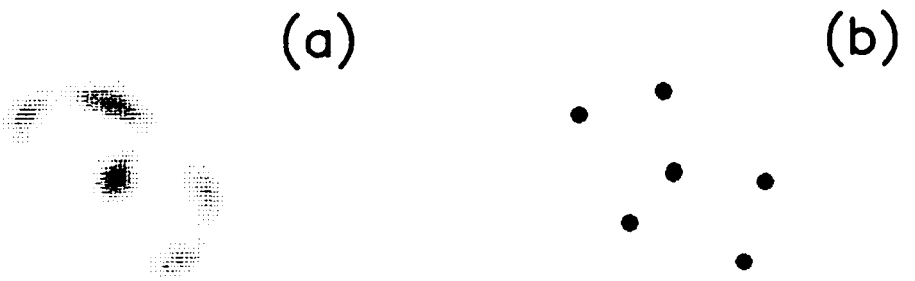

Figure 6: Planar configuration of six ions for $\nu_z = 0.780$ MHz and $\nu_r = 0.347$ MHz. Five ions are presumed to lie at the vertices of a pentagon in the x-y plane, but one does not fluoresce. Another one lies at the origin. (a) Experimental data. (b) Calculation.

$\nu_z = 0.439$ MHz and $\nu_r = 0.304$ MHz. The ions in Fig. 7 lie in the x-y plane. This configuration is the same as the calculated one shown in Fig. 1 of Ref. 3. The outer ring of the experimental image appears to be incomplete in this case because of nonuniform illumination of the cluster by the tightly focused 194 nm beam. In Fig. 8, two ions lie along the z axis, symmetrically above and below the x-y plane. The others form a ring in the x-y plane. The number of ions in Figs. 7 and 8 was determined uniquely from the observed configurations for the two different sets of conditions.

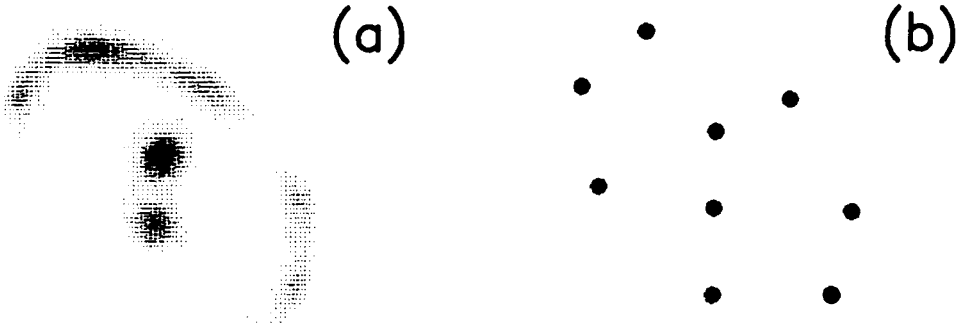

Figure 7: Planar configuration of nine ions for $\nu_z = 0.497$ MHz and $\nu_r = 0.256$ MHz. (a) Experimental data. (b) Calculation.

Figure 9 shows 15 ions for $\nu_z = 0.780$ MHz and $\nu_r = 0.347$ MHz. All of them lie in the x-y plane. Five form a pentagon, and the other ten form the outer ring. The observed pattern is only consistent with the one calculated for 15 ions.

Figure 10 shows 16 ions, for $\nu_z = 0.626$ MHz and $\nu_r = 0.479$ MHz. The large ring of eight ions lies nearly in the x-y plane. Two smaller rings of four ions each are displaced along the z axis, above and below the x-y plane. If another ion is added, at the same trap voltages, then, according to calculations, one ion goes to the center. By using data taken at another set of trap voltages, we could determine the number of ions. The 16 ions lie close to the surface of a spheroid. For larger numbers of ions, one would expect to see a

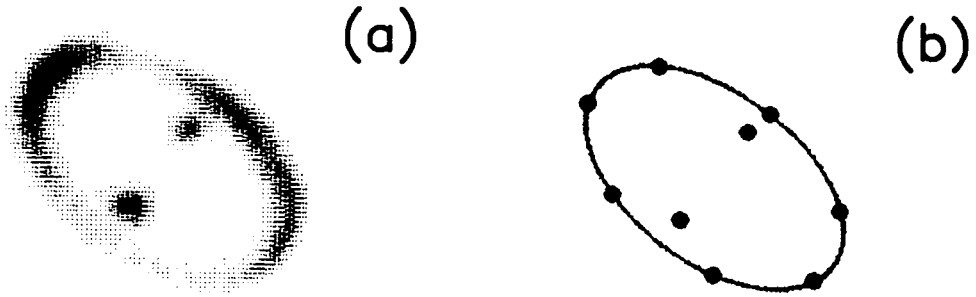

Figure 8: Nonplanar configuration of nine ions for $\nu_z = 0.439$ MHz and $\nu_r = 0.304$ MHz. Seven circulate in the x-y plane. The other two are displaced along the z axis. (a) Experimental data. (b) Calculation.

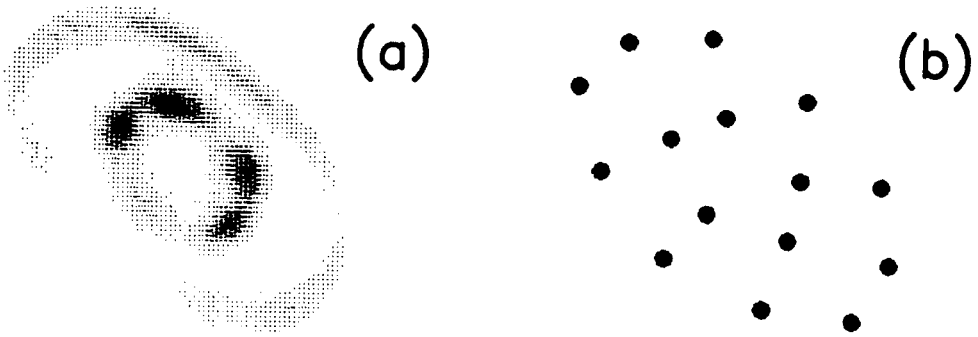

Figure 9: Planar configuration of 15 ions for $\nu_z = 0.780$ MHz and $\nu_r = 0.347$ MHz. (a) Experimental data. (b) Calculation.

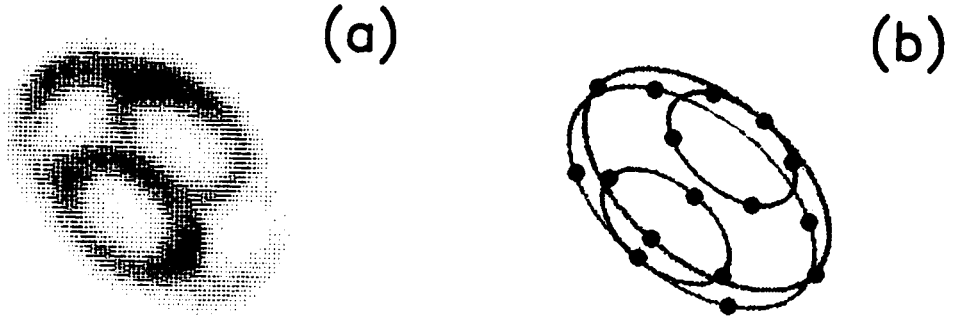

Figure 10: Nonplanar configuration of 16 ions for $\nu_z = 0.626$ MHz and $\nu_r = 0.479$ MHz. (a) Experimental data. (b) Calculation.

series of concentric spheroids like those which have been predicted and observed in Penning traps.[12,25]

VI. Related physical systems

A. Macroscopic particle traps

Perhaps the earliest studies of spatially ordered systems of charged particles in a Paul trap were made by Wuerker, Shelton, and Langmuir about 30 years ago.[24] In these studies, aluminum particles that had diameters of a few micrometers were suspended in a large Paul trap and cooled by collisions with gas molecules.

A similar trap has been built in our laboratory.[10] The inner diameter of the ring was about 2.5 cm. Typical trap parameters were $V_0 \approx 350$ V, $U_0 \approx 0$ V, and $\Omega/2\pi \approx 60$ Hz. Aluminum oxide particles of approximate mass 10^{-9} g and charge approximately 10^5 times the proton charge were trapped and observed to form ordered structures.

B. The Thomson model of the atom

In an early model for the atom, first suggested by Kelvin and later studied in detail by Thomson, electrons were assumed to be embedded in a uniform sphere of positive charge.[26] The potential energy of an electron inside the sphere due to the positive charge is proportional to $x^2 + y^2 + z^2$. Thus, the stable spatial configurations of the electrons in such a model are the same as for ions in a Paul trap with a spherically symmetric effective potential. Thomson's calculations of the minimum-energy configurations, which actually were done in two dimensions, showed patterns of concentric rings. He tabulated the configurations for up to 100 electrons. The 100-electron configuration contains seven rings. For $\nu_z > \nu_r$, the three-dimensional configurations for small numbers of particles are the same as for Thomson's two-dimensional calculations. For example, Thomson's 15-electron configuration has five in the inner ring and ten in the outer ring, like the data of Fig. 9. Thomson's calculations are perhaps the earliest predictions of layered structures in a bound Coulomb system. Such layered structures are predicted to occur in one-, two-, and three-dimensional systems[25] and have been observed in the Penning trap, a three-dimensional system.[12]

Thomson discussed experiments with floating magnets, which he used to verify his calculations of the two-dimensional configurations. For these experiments, equally magnetized needles, oriented in the same way, were pushed through corks and floated on water. An attractive force was produced by a large magnet placed above the surface of the water, the lower pole having the opposite sign to that of the upper poles of the floating magnets.

VII. Discussion

The equilibrium shapes of clusters that contain 16 ions or fewer and the intra-cluster vibrational frequencies can be calculated from the effective potential approximation. Other properties, however, such as the Doppler spectrum or the order-chaos transition, are affected by the micromotion, and require a more complete theoretical treatment.

Experiments with charged micrometer-sized particles in Paul traps might be useful in testing calculations, since they are relatively simple to perform, compared to experiments with ions. Large numbers of particles (on the order of 100) can be cooled and optically observed. The melting and freezing phase transitions have been observed previously.[24] Perhaps further experimental work could reveal details of the transition to chaotic behavior.[8,9] Other kinds of traps, with linear or "racetrack" geometries[27] might be useful in simulating ordered structures in ion storage rings. Such structures have been predicted, but not yet observed.[28]

Acknowledgments

We gratefully acknowledge support from the Air Force Office of Scientific Research and the Office of Naval Research.

References

1. J. Mostowski and M. Gajda, Acta Phys. Pol. **A67**, 783 (1985).
2. E. V. Baklanov and V. P. Chebotayev, Appl. Phys. B **39**, 179 (1986).
3. J. Javanainen, J. Opt. Soc. Am. B **5**, 73 (1988).
4. R. Casdorff and R. Blatt, Appl. Phys. B **45**, 175 (1988).
5. J. D. Prestage, M. J. Djomehri, and L. Maleki, Bull. Am. Phys, Soc. **33**, 914 (1988).
6. F. Diedrich, E. Peik, J. M. Chen, W. Quint, and H. Walther, Phys. Rev. Lett. **59**, 2931 (1987).
7. D. J. Wineland, J. C. Bergquist, W. M. Itano, J. J. Bollinger, and C. H. Manney, Phys. Rev. Lett. **59**, 2935 (1987).
8. J. Hoffnagle, R. G. DeVoe, L. Reyna, and R. G. Brewer, Phys. Rev. Lett. **61**, 255 (1988).
9. R. Blümel, J. M. Chen, E. Peik, W. Quint, W. Schleich, Y. R. Shen, and H. Walther, Nature **334**, 309 (1988).
10. D. J. Wineland, W. M. Itano, J. C. Bergquist, S. L. Gilbert, J. J. Bollinger, and F. Ascarrunz, in *Non-neutral Plasma Physics*, edited by C. W. Roberson and C. F. Driscoll, A. I. P. Conf. Proc. **175**, (Am. Inst. Phys., New York, 1988), p. 93.
11. P. Toschek et al., these Proceedings.
12. S. L. Gilbert, J. J. Bollinger, and D. J. Wineland, Phys. Rev. Lett. **60**, 2022 (1988).
13. W. M. Itano, J. C. Bergquist, R. G. Hulet, and D. J. Wineland, Phys. Rev. Lett. **59**, 2732 (1987).
14. J. C. Bergquist, D. J. Wineland, W. M. Itano, H. Hemmati, H.-U. Daniel, and G. Leuchs, Phys. Rev. Lett. **55**, 1567 (1985).

15. E. C. Beaty J. Appl. Phys. **61**, 2118 (1987).

16. H. Hemmati, J. C. Bergquist, and W. M. Itano, Opt. Lett. **8**, 73 (1983).

17. W. M. Itano, J. C. Bergquist, and D. J. Wineland, Science **237**, 612 (1987); D. J. Wineland and W. M. Itano, Phys. Today **40** No. 6, 34 (1987).

18. H. G. Dehmelt, Bull. Am. Phys. Soc. **20**, 60 (1975).

19. D. J. Wineland and W. M. Itano, Phys. Lett. **82A**, 75 (1981).

20. R. H. Dicke, Phys. Rev. **89**, 472 (1953).

21. D. J. Wineland and W. M. Itano, Phys. Rev. A **20**, 1521 (1979).

22. J. C. Bergquist, W. M. Itano, and D. J. Wineland, Phys. Rev. A **36**, 428 (1987).

23. W. H. Press, B. P. Flannery, S. A. Teukolsky, and W. T. Vetterling, *Numerical Recipes* (Cambridge Univ. Press, London, 1986).

24. R. F. Wuerker, H. Shelton, and R. V. Langmuir, J. Appl. Phys. **30**, 342 (1959).

25. A. Rahman and J. P. Schiffer, Phys. Rev. Lett. **57**, 1133 (1986); D. H. E. Dubin and T. M. O'Neil, *ibid.* **60**, 511 (1988); J. P. Schiffer, *ibid.* **61**, 1843 (1988).

26. J. J. Thomson, Phil. Mag. **7**, 237 (1904); *The Corpuscular Theory of Matter* (Scribner's Sons, New York, 1907).

27. D. A. Church, J. Appl. Phys. **40**, 3127 (1969).

28. J. P. Schiffer and P. Kienle, Z. Phys. A **321**, 181, (1985); J. P. Schiffer and O. Poulsen, Europhys. Lett. **1**, 55 (1986); D. Habs, in *Lecture Notes in Physics 296*, edited by M. Month and S. Turner (Springer-Verlag, Berlin, 1988), p. 310.